JOURNAL OF AGRICULTURAL AND FOOD CHEMISTRY

Aggregation of a Proline-Rich Protein Induced by Epigallocatechin Gallate and Condensed Tannins: Effect of Protein Glycosylation

CHRISTINE PASCAL,[†] CÉLINE PONCET-LEGRAND,[†] BERNARD CABANE,[‡] AND AUDE VERNHET*,[§]

INRA and Montpellier SupAgro, UMR1083, Sciences Pour l'Œnologie, 2 place Pierre Viala, F-34060 Montpellier, France, and Laboratoire PMMH, CNRS−ESPCI, 10 rue Vauquelin, 75231 Paris Cedex 05, France

Astringency is one of the most important organoleptic qualities of numerous beverages, including red wines. It is generally thought to originate from interactions between tannins and salivary proline-rich proteins (PRPs). In this work interactions between a glycosylated PRP, called II-1, and flavan-3-ols were studied in aqueous solutions and at a colloidal level, by dynamic light scattering (DLS) and small-angle X-ray scattering (SAXS). The flavan-3-ols were a monomer, epigallocatechin gallate (EGCG), and polymerized flavan-3-ol fractions extracted from grape seeds. In aqueous solutions containing EGCG and protein II-1, protein aggregation took place when protein concentration and the EGCG/protein ratio exceeded a threshold. The aggregates had a small size, comparable with the dimensions of protein monomers, and formed stable dispersions (no phase separation). Most proteins remained free in solution. This behavior is in sharp contrast with the phase separation observed for nonglycoslated PRP in the same conditions. Moreover, this slight aggregation of II−I in the presence of EGCG was disrupted by the addition of 12% ethanol. Increasing the flavan-3-ol molecular weight strongly enhanced II−I/tannin aggregation: the threshold was at a lower protein concentration (0.2 mg/mL) and a lower tannin/protein ratio. Still, in most cases, and in contrast with that observed with a nonglycosylated PRP, the aggregates remained of discrete size and stable. Only at low ethanol content (2%) did the addition of tannin polymers finally lead to phase separation, which occurred when the molar ratio of tannins to proteins exceeded 12. This systematic effect of ethanol confirmed the strong effect of cosolvents on protein/tannin interactions.

KEYWORDS: Proline-rich proteins; glycosylation; flavan-3-ols; EGCG; small-angle X-ray scattering; dynamic light scattering

INTRODUCTION

Tannins are considered as a part of the plant defense system against environmental stressors. For example, they can provide defense against microbial attacks and make food unpalatable to predators (*1*). They have a large number of effects on animals, including inhibition of digestive enzymes and growth rate depression (*2*). These biological effects are related to the ability of tannins to interact with proteins and sometimes to precipitate them (*3*). The parotid saliva of herbivorous and omnivorous mammals, including humans, contains proline-rich proteins (PRPs), whereas these proteins are absent from the saliva of carnivores (*2, 4*). PRPs have a high affinity for tannins and there is some evidence that this affinity constitutes a mean of protection against the deleterious dietary effects of these polyphenols (*2, 5*). Interactions between tannins and PRPs are also thought to be at the origin of astringency. This oral sensation is felt when eating or drinking plant-based foods (chocolate) and beverages (tea, beer, cider, wine). It was described by the American Society for Testing and Materials as a "complex of sensations due to shrinking, drawing or puckering of epithelium as result of exposure to substances such as alums or tannins" (*6*). These sensations are usually attributed to friction-based mechanisms induced by salivary protein precipitation (*7*). Precipitates themselves may be sensed as discrete particles and/or cause a loss of lubrication of the oral epithelium, possibly as a result of loss of viscosity (*8–14*).

PRPs, which constitute about two-thirds of human parotid salivary proteins (*4, 15*), are usually divided into glycosylated, acidic and basic types, which have widely different functions (*16*). Acidic PRPs are reported to bind calcium and to inhibit crystal growth, functions that may be important in maintaining

* Corresponding author: tel +33 499 612 758; fax +33 499 612 857; e-mail vernhet@supagro.inra.fr.
[†] INRA, UMR 1083, Sciences Pour l'Œnologie.
[‡] Laboratoire PMMH, CNRS−ESPCI.
[§] Montpellier SupAgro, UMR 1083, Sciences Pour l'Œnologie.

10.1021/jf800790d CCC: $40.75
Published on Web 07/19/2008

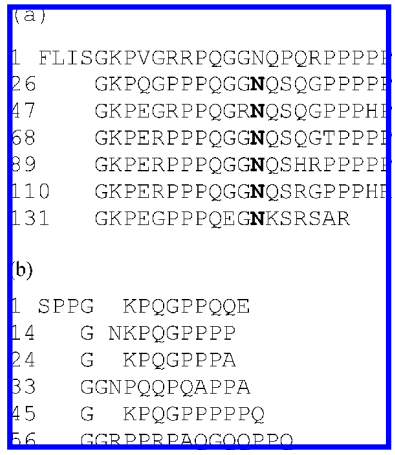

Figure 1. Sequences of the recombinant PRPs (**a**) II-1 and (**b**) IB-5, from ref *28*. This presentation emphasizes the tandem repeats. Potential glycosylation sites are indicated in boldface type.

calcium homeostasis in the mouth (*3*). They are also involved in dental pellicle formation. The only known biological function of basic PRPs is to interact with plant tannins (*17*), constituting a means of protection against the harmful effects of these polyphenols (*2*). Glycosylated PRPs bind oral bacteria (*18*) and ensure oral lubrication (*19*). If astringency is related to a reduction of saliva viscosity, this last class of PRP may therefore be more implicated in this sensation than the other two. Understanding factors that affect interactions between tannins and salivary proline-rich proteins, and the consequences of these interactions, will contribute to elucidate the exact physiological mechanisms implied in astringency. Many studies have been devoted to the study of the interactions between nonglycosylated proline-rich proteins or peptides and polyphenols. The formation of insoluble complexes has been thoroughly investigated (*20–24*) and several techniques have been used to study these interactions at a molecular level (*13, 14, 17, 25, 26*). Fewer papers concern glycosylated PRPs (*5, 27*).

Two human salivary PRPs, one glycosylated and the other not, were produced by the recombinant pathway, as described before (*28*). The glycosylated PRP is similar to a human salivary PRP called II-1 (**Figure 1**). Its glycosyl moiety is composed of 98% mannose and 2% glucose. II-1 molecular weight was estimated to be 20 700 and its isoelectric point is 11.9. The nonglycosylated PRP is similar to IB-5 (**Figure 1**), another human salivary PRP. The molecular weight of IB5 is 7000 and its isoelectric point is 11.2. Both PRPs contain tandem repeats in their amino acid sequences and are natively unfolded. In the present work, interactions between the glycosylated PRP II-1 and flavan-3-ols were studied by dynamic light scattering (DLS) and small-angle X-ray scattering (SAXS). A monomer, epigallocatechin gallate (EGCG), was first used as a model flavan-3-ol. Results were compared to those previously obtained on the interactions between the non-glycosylated protein IB-5 and EGCG (*29*). Procyanidin fractions extracted from grape seeds were used in a second experiment. Indeed, our interest mainly concerns the astringency of red wines, which is of primary importance for their mouth-feel assessment. Tannins in red wines are oligomers and polymers of flavan-3-ol units primarily linked by C4−C8 bonds, C4−C6 bonds giving rise to varying degrees of polymer branching (**Figure 2**) (*30, 31*). The constitutive units of grape seed tannins are (+)-catechin (C), (−)-epicatechin (EC), and (−)-epicatechin-gallate (EC-G). In grape skin tannins (−)-epigallocatechin (EGC) is also present, accounting for about 30% of the units. Experimental conditions were similar to enological conditions: an aqueous solvent was used with an ionic

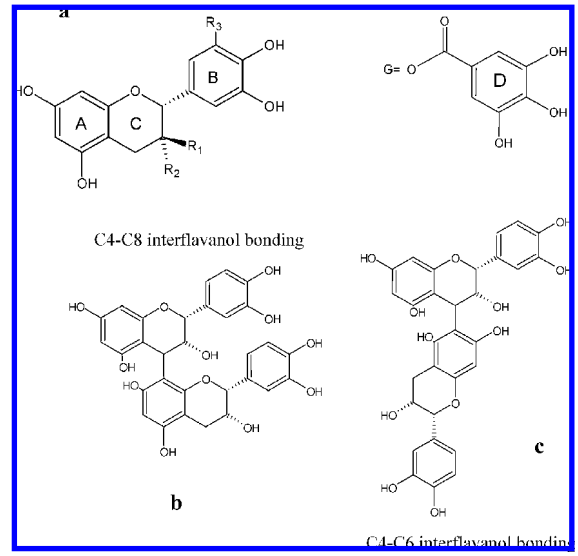

Figure 2. Structures of (**a**) flavan-3-ol monomers and (**b**, **c**) condensed tannins (dimers). (**a**) For catechin (C), R1 = OH and R2 = R3 = H; for epicatechin (EC), R1 = R3 = H and R2 = OH; for epigallocatechin (EGC), R1 = H and R2 = R3 = OH; for epicatechin gallate (EC-G), R1 = R3 = H and R2 = G; for epigallocatechin gallate (EGC-G), R1 = H, R2 = G, and R3 = OH; G = gallic acid. (**b, c**) C4−C8 and C4−C6 interflavanol bonding.

strength and a pH set in the wine range (*4, 32*). The influence of ethanol as a cosolvent was also investigated.

MATERIALS AND METHODS

Materials: Chemical. EGCG was purchased from Sigma−Aldrich (St. Louis, MO); sodium hydroxide, hydrochloric acid, and sodium chloride were from Merck (Whitehouse Station, NJ).

Glycosylated Proline-Rich Protein. Human salivary PRPs were produced by use of the yeast *Pichia pastoris* as a host organism and purified as described previously (*28*). The glycosylated protein N-terminal sequence corresponded to the II-1 sequence without its first 11−13 amino acids. As there is no proline residue in the first 13 amino acids of the cloned sequence, the recombinant protein's physicochemical properties should not be very different from those of the naturally occurring protein. The glycosyl moiety was estimated to represent 22% of the molecular weight of II-1 [average from monosaccharide assay after trimethylsilylation (TMS) of polysaccharides (*33*) and aldolization methods (*34*)]. It is mainly composed of mannose and glucose. Considering the amino acid sequence of the protein and the polysaccharide percentage, we estimated the molecular weight of II-1 to be 20 700. This average molecular weight was used to evaluate the EGCG to protein molar ratio. Nevertheless, in this paper, the concentration of the protein II-1 will always be indicated in milligrams per milliliter because of the uncertainty on the protein molecular weight.

Tannins. Polymerized flavan-3-ol fractions were purified from grape seeds (*Vitis vinifera* var Chiraz) following the procedure described elsewhere (*35*). These fractions were analyzed by thiolysis followed by HPLC, as described previously (*30, 31*). This allowed the determination of their mean degree of polymerization (mDP) and of their percentage of galloylation (of epicatechin-gallate units). It must be emphasized that thiolysis gives the mean molecular weight of the fraction but does not provide any information about polymer size distribution. Two fractions were used: a fraction of mDP 4 with 14% galloylation, and a fraction of mDP 15 with 20% galloylation.

Sample Preparation. Stock solutions of proteins (1−5 mg/mL) and of EGCG (4 or 8 mM) were prepared by dissolving the freeze-dried protein in a 100 mM NaCl solution acidified to pH 3.5 with HCl, with or without 12% (v/v) ethanol. This pH was chosen because it is representative of wine. We also checked that this pH is not strongly modified by saliva when drinking wine. NaCl was added to the solutions at a final concentration of 100 mM to produce ionic strengths on the

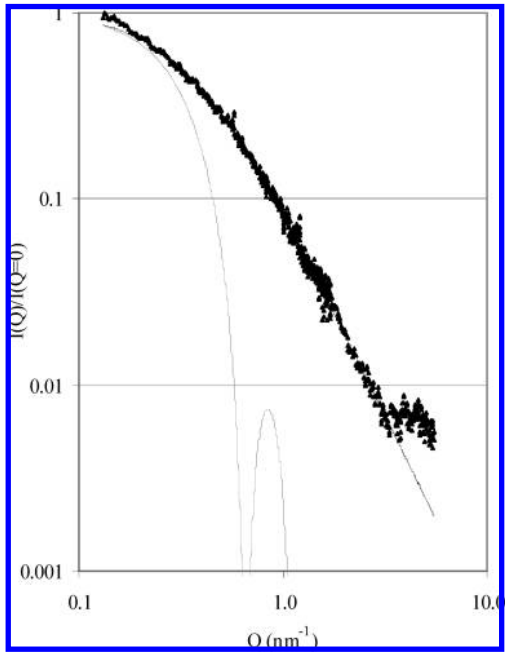

Figure 3. SAXS spectrum of the glycosylated protein II-1 alone at 3 mg/mL in water + 100 mM NaCl in a log I − log Q representation. The dark line is the fit by the Fisher−Burford function that describes self-similar objects with a fractal dimension $d_f = 2.2$ and a gyration radius of 5.3 nm. The gray line is the fit by the form factor of spheres with the same gyration radius.

order of those of saliva (*36*) and wine (*32*). These stock solutions were immediately frozen (− 20 °C) to prevent EGCG oxidation and protein proteolysis. Prior to use, stock solutions were diluted to the required concentration. Their pH was checked and adjusted with 1 N HCl when necessary, and they were filtered with disposable syringe filters [Millipore, poly(vinylidene difluoride) (PVDF) membrane, 0.22 μm].

To ensure their dissolution, grape seed tannins were initially dissolved in absolute ethanol (*35*), to a maximum concentration of 12 mg/mL. These stock solutions were then further diluted in ethanol and/or in model solutions to obtain the required tannin concentration and solvent composition [100 mM NaCl, pH 3.5, and 2% or 12% (v/v) ethanol].

Dynamic Light Scattering. Interactions between protein and flavan-3-ols (EGCG or seed tannins) were monitored with a Malvern Autosizer 4800 (Malvern Instruments, Malvern, U.K.) equipped with a 35 mW He−Ne laser (λ = 633 nm, Coherent, Auburn, CA). Measurements were carried out at 25 °C, at an angle of 90° from the incident beam. Equal volumes of flavan-3-ol and protein solutions, at a concentration that was twice the desired final concentration, were mixed in the measurement cell (time zero). The mixture was then monitored for several hours through measurements of the scattering intensity and of the autocorrelation function $G(t)$ of the scattered light. Each measurement was the average of 10 replicates. Control measurements were performed on solvents and on proteins, EGCG, and tannin solutions at the adequate concentrations. A rise in scattered intensity above that of the controls indicated the onset of aggregation. The autocorrelation function of the scattered light was first analyzed by the cumulant method. With this method, the logarithm of the normalized correlation function is first fitted to a polynomial:

$$\log\left[\frac{G(t)}{B} - 1\right] = a + bt + ct^2 + \ldots \quad (1)$$

where $G(t)$ are the measured correlation points, B is the baseline, and a, b, and c are the coefficients of the cumulant fit determined by a simple linear least-squares fitting procedure. a is referred to as the intercept, while the slope b measures the relaxation time for the signal. The diffusion coefficient D of the colloids can be calculated as

$$\frac{1}{b} = 2DK^2 \quad (2)$$

where $K = (4\pi n_0/\lambda)\sin(\theta/2)$ is the scattering vector, n_0 is the solvent refractive index, λ is the laser wavelength, and θ is the scattering angle. The polydispersity index PI, defined as $c/2b$, measures the variance (standard deviation squared) of the distribution of particle size.

The mean hydrodynamic radii of the particles, R_h, are then derived from the diffusion coefficient D by use of the Stokes−Einstein equation with the assumption of spherical shapes:

$$D = kT/(6\pi\eta R_h) \quad (3)$$

where k is the Boltzmann constant, T is the temperature, and η is the solvent viscosity. Cumulant analysis of $G(t)$ then provides the mean hydrodynamic diameter D_h of the particles, in nanometers and weighted according to the scattered intensity I_s, and the polydispersity index PI of the suspension ($0 < PI < 1$). The intensity scattered by a particle is strongly dependent on its size ($I \propto R_h^6$). Thus, for polydisperse samples, the mean hydrodynamic diameter D_h weighted according to I_s is in favor of the largest particles and is overestimated. For polydispersity indexes above 0.2, autocorrelation functions were also analyzed by use of the Contin algorithm to obtain information on particle size distribution (*37*). The size distribution is then divided into a series of size classes and the percentage of the size distribution in each size class is calculated. Results are expressed as mean hydrodynamic diameters weighted according to the intensity, the volume, or the number. The scattered intensity, expressed in kC, is given for a pinhole of 100 μm.

Small-Angle X-ray Scattering. SAXS experiments were performed on the BM2-D2AM beam line at the European Synchrotron Radiation Facility (ESRF, Grenoble, France). The incident beam (energy 16 keV) was directed with point collimation onto the sample, and the scattered X-rays were counted by a charge-coupled device (CCD) camera located either at 1.6 m or at 0.27 m from the sample. The scattered intensities were then radially averaged and sorted according to the magnitude of the scattering vector Q:

$$Q = \frac{4\pi}{\lambda}\sin\left(\frac{\theta}{2}\right) \quad (4)$$

Spectra were recorded over a range of Q values that extended from 0.08 to 2.3 nm^{-1} (long collimation) and from 0.5 to 8 nm^{-1} (short collimation), corresponding to real-space distances between 0.8 and 80 nm. Each spectrum was recorded with a 50 s irradiation time. The absence of irradiation damage was checked by comparison with shorter and longer irradiation times. Spectra of the solvents, the proteins, and the EGCG solutions, at their highest concentrations, were recorded first. The initial concentrations of the protein solutions were set at 1 and 3 mg/mL. Then small volumes of a concentrated EGCG solution were progressively added to the protein solutions in the measurement cell so as to obtain a progressive increase of the EGCG/protein ratio. SAXS spectra were recorded after each addition.

The SAXS data were analyzed according to classical formulas for the scattering from dispersions of particles or macromolecules in a homogeneous solvent. For such dispersions, the intensity per unit volume can be decomposed as a product of the intensity scattered by a single particle and a structure factor that describes the interferences between rays scattered by different particles (*38*):

$$I(Q) = N_p(\rho_p - \rho_s)^2 V_p^2 P(Q) S(Q) \quad (5)$$

where ρ_p is the scattering length density of the particles and ρ_s is that of the solvent, V_p is the volume of a particle, N_p is the number of particles per unit volume, $P(Q)$ is the form factor of particle, and $S(Q)$ is the structure factor that describes the pair correlations between the positions of all particles. If the sample is a dilute dispersion, where the relative positions of the particles are not correlated, then $S(Q) = 1$ at all Q values. The general features of the scattering curves for independent particles dispersed in a homogeneous liquid are as follows.

(a) As $Q \to 0$, the particle form factor is $P(Q) = 1$. Hence, the intensity is proportional to the average volume V_p per particle multiplied by their volume fraction $\phi_p = C_p/d_p$, where C_p is the mass concentration of particles and d_p is the mass per unit volume of one particle:

$$I(Q \to 0) = (\rho_p - \rho_s)^2 \phi_p V_p \quad (6)$$

(b) At finite Q values, the rays scattered by nuclei at opposite ends of a particle interfere destructively. In this regime, the curvature of the scattering curve measures the average radius of gyration, R_g, of the particles. This quantity may be determined by fitting the measured intensity curve to the Guinier approximation (*39*), valid for $QR_g < 1$:

$$P(Q) = P(Q \to 0) \exp\left(-\frac{Q^2 R_g^2}{3}\right) \quad (7)$$

(c) At higher Q values, the intensity decay reflects interferences at shorter distances within each particle, that is, their internal structure. For homogeneous spherical particles of outer radius R, the equation of the scattering curve is

$$P(QR) = \left[\frac{3(\sin QR - QR \cos QR)}{(QR)^3}\right]^2 \quad (8)$$

At high Q values, this function oscillates around a Q^{-4} decay, which is the general Porod's law for homogeneous globular particles. For globular particles, we have used the calculated scattering curves of polydisperse spheres, by summing over the scattering curves of individual spheres weighted by their volumes and concentrations. This has the effect of damping the oscillations at high Q values.

For particles that are not globular we have used the Fisher−Burford approximation, which describes particles that have a radius of gyration R_g and a self-similar structure characterized by an exponent d_f. At high Q values, this function merges to a Q^{-d_f} decay:

$$P(QR_g) = \left[1 + \frac{(QR_g)^2}{3d_f/2}\right]^{-d_f/2} \quad (9)$$

RESULTS AND DISCUSSION

Colloidal Stability of the II-1/EGCG Mixtures. In a first step, DLS was used to explore the composition map of the aqueous solutions containing protein II-1 and EGCG. This was motivated by previous reports on solutions of nonglycosylated protein IB-5 (*29*) and related peptides (*17*), which indicate that for these components EGCG causes continuous aggregation and phase separation when the concentrations of both solutes exceed a threshold.

Solutions containing low concentrations of protein II-1 (0.20 mg/mL) gave low scattered intensities at all EGCG concentrations up to 0.88 mg/mL, which corresponds to an EGCG/protein molar ratio on the order of 200/1. Moreover, scattering intensities did not change over 24 h. Accordingly, no protein aggregation could be detected on this time scale. At higher protein concentrations (1 mg/mL), EGCG addition at a concentration of 1.83 mg/mL (EGCG/protein molar ratio 80/1) caused a slight increase in the scattered intensity. Analysis of the intensity correlation function indicated that the scattering was produced by a heterogeneous population of aggregates (polydispersity index 0.4) with a mean hydrodynamic diameter, weighted according to the number, on the order of 20 nm. The scattering intensity only evolved slowly over 24 h, and neither precipitation nor any other kind of phase separation was observed. Accordingly, EGCG caused some protein aggregation at high protein concentrations, but this aggregation was limited.

SAXS Experiments. These experiments were performed at higher concentrations to obtain more precise information on these aggregation processes. SAXS spectra were first recorded for the pure solutions of EGCG in 100 mM NaCl (pH 3.5). At their highest concentration (2.64 mg/mL), the pure EGCG solutions gave a scattering that was weak and independent of the scattering vector Q. Accordingly, EGCG did not self-associate at these concentrations.

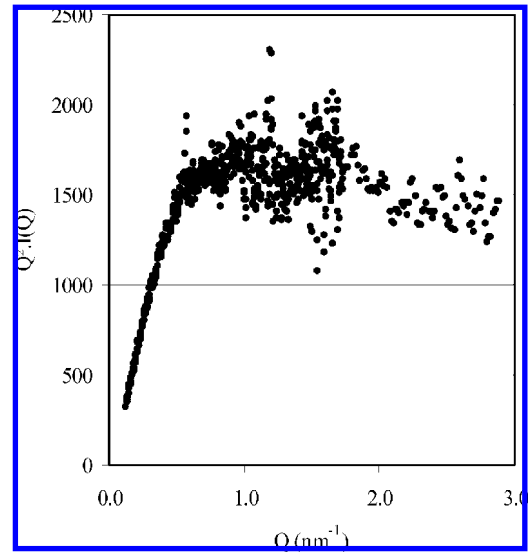

Figure 4. SAXS spectrum of the glycosylated protein II-1 alone at 3 mg/mL in water + 100 mM NaCl in the Kratky representation $Q^2I(Q)$ vs Q. The plateau of $Q^2I(Q)$ for $0.6 < Q < 3$ nm^{-1} is characteristic of unstructured proteins.

SAXS spectra were also obtained with pure solutions of protein II-1 at different concentrations (1 and 3 mg/mL). These spectra, shown here for a protein concentration of 3 mg/mL (**Figure 3**), were typical of the scattering by noninteracting flexible polymers. Indeed, the asymptotic decay of the intensity followed a Q^{-2} power law, as opposed to the Q^{-4} power law that is obeyed by the scattering from dense particles. This is evident in **Figure 4**, where the scattering is presented in the Kratky representation, since the values of $Q^2I(Q)$ remain constant within experimental uncertainties from $Q = 0.6$ nm^{-1} to $Q = 3$ nm^{-1}. The Q^{-2} power law is a signature of flexible noninteracting polymers such as natively unstructured proteins (*40, 41*) and is in accordance with the nature of protein II-1.

Quantitative structural information can be extracted from fits of the experimental spectra by the scattering curves of known objects. As expected, the scattering curve for polydisperse spheres (eq 8) bears no resemblance to the experimental spectra. On the other hand, good fits were obtained with the scattering curves of self-similar objects with a fractal dimension close to $d_f = 2.2$, for instance, the Fisher−Burford approximation (eq 9). This fit yields a radius of gyration R_g on the order of 5.3 ± 0.1 nm, which corresponds to an end-to-end distance of 12 nm. This radius is quite large compared with those of globular proteins: for instance, lysozyme (molar mass 14.3 kDa) has a radius of gyration of only 1.3 nm. It is more in line with the radii of proteins that are intrinsically unfolded, such as the PIR domain of Grb14, studied by Moncoq et al. (*41*), which has a radius of 2.7 ± 0.1 nm for a molar mass of only 7.9 kDa.

Next, a concentrated EGCG solution was progressively added to the less concentrated protein solution (1 mg/mL). This resulted in a progressive dilution of the protein in the mixture. The highest EGCG concentration was 1.34 mg/mL and the corresponding protein concentration was 0.73 mg/mL (EGCG/protein molar ratio 82/1). These mixed solutions gave spectra that were identical with that of the protein alone (results not shown). Therefore protein aggregation did not occur under these conditions, or it was too slow to be observed during the length of the experiment, or the number of aggregates was too small to give substantial scattering.

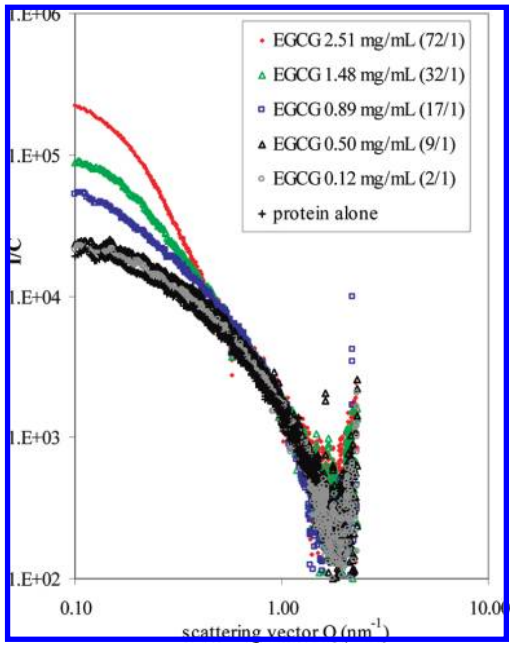

Figure 5. Effect of EGCG additions to the solutions of the glycosylated protein II-1 in water + NaCl 100 mM. The SAXS spectra are presented as intensity divided by the protein concentration, *I*/*C*, vs scattering vector *Q* in log−log scales. The EGCG concentrations in the mixture are, from top to bottom, 2.51, 1.48, 0.89, 0.50, 0.12, and 0 mg/mL. The corresponding protein concentrations are 1.6, 2.1, 2.4, 2.6, 2.8, and 3 mg/mL and the EGCG/protein molar ratios are 72/1, 32/1, 17/1, 9/1, 2/1, and 0, respectively. For the lower ratios, up to 9/1, the values of *I*/*C* are unchanged. For the higher ratios (17/1 and above), there is an abrupt increase in the scattered intensity at low *Q* values, indicating that the proteins are aggregated by EGCG.

For a similar molar ratio (80/1) and a slightly higher protein concentration (1 mg/mL), only a small signal could be observed by DLS, indicating that aggregation was limited. Note that adsorption of some EGCG molecules to the proteins could have taken place without causing any substantial changes to the protein scattering, since the molar mass of EGCG is quite small compared to that of II-1.

Finally, EGCG was added to the aqueous solution of protein II-1 made at the higher concentration (3 mg/mL). In this case, there was a strong increase in the intensity scattering at low *Q*, but only when the EGCG concentration exceeded a threshold. The magnitude of this excess intensity kept growing with the EGCG/protein ratio (**Figure 5**). According to eq 4, a higher intensity scattering at low *Q* indicates that the objects that scatter the X-rays at low *Q* have a larger volume and a larger mass; that is, protein/EGCG aggregates have formed. Moreover, the excess scattering at low *Q* has the same steep decay as the scattering of globular objects, such as dense spheres. Hence the aggregates must be dense objects, in contrast to the protein monomers. A fit of scattering at low *Q* by the scattering curves of polydisperse spheres indicates that the radius of these spheres remains close to 10 nm, even when the EGCG/protein ratio increased. Despite these changes at low *Q* values, the scattering at high *Q* remained close to that of the pure protein solutions (in units of intensity/protein concentration). This intensity must originate from proteins that are nonaggregated. The full spectrum may then reflect the coexistence of proteins/EGCG aggregates with nonaggregated proteins. Since the high *Q* scattering remains nearly the same at high EGCG/protein molar ratios, when aggregates are formed, we must conclude that the formation of the aggregates does not significantly deplete the concentration of protein monomers. Note that the solutions made at lower protein concentrations did not aggregate at the same EGCG/protein concentration ratios, or even at higher ones. Therefore the threshold for aggregation must be related to protein concentration as well as to EGCG/protein ratio.

These results cannot be explained by a simple association equilibrium in which a single protein (P) would bind individual EGCG molecules (T) with binding constants *K*, such as

$$\mathrm{P} + n\mathrm{T} \Leftrightarrow \mathrm{PT}_n \qquad (10)$$

Indeed, such an equilibrium would cause a slow and continuous rise of scattered intensity at all concentrations, rather than the abrupt increase shown in **Figure 5** for EGCG concentrations that exceed the threshold. Nor can these results be explained by an open-ended association equilibrium such as

$$\mathrm{P} \Leftrightarrow \mathrm{PT} \Leftrightarrow \mathrm{PPT} \Leftrightarrow \mathrm{PPTT} \Leftrightarrow \mathrm{PPPTT} \Leftrightarrow \ldots \qquad (11)$$

Indeed, this would yield aggregates of ever-increasing sizes, which would eventually precipitate out of solution, rather than the finite-sized aggregates (radius = 10 nm) observed here. Instead, these results indicate that the objects detected through scattering result from a closed aggregation equilibrium, in which *m* proteins and *n* tannins associate to form one aggregate:

$$m\mathrm{P} + n\mathrm{T} \Leftrightarrow \mathrm{P}_m\mathrm{T}_n \qquad (12)$$

If the association constant K_m that describes this equilibrium is large, this equilibrium will be similar to a micellization equilibrium, which is well-known to produce aggregates of finite sizes (the micelles) at concentrations that exceed a threshold (the critical micelle concentration). The location of the threshold with respect to protein concentration and EGCG/protein ratio must be determined by the values of *m*, *n*, and K_m. Finally, if *K* is small and K_m is large, this model will cause to the aggregates (protein−tannin aggregates) to coexist with a large population of free proteins, as observed in the SAXS spectra taken at concentrations that exceed the threshold (**Figure 5**).

Effect of Ethanol on EGCG/II-1 Interactions. Interactions between flavan-3-ols and proteins are generally attributed to hydrophobic interactions between the aromatic rings of the tannins and hydrophobic sites of the protein, strengthened by hydrogen bonding between the H-acceptor sites of the proteins and the hydroxyl groups carried by polyphenols (*13, 24, 42–46*). With proline-rich proteins, the proline units are considered as the main interaction sites between polyphenols and proteins: the pyrrolidine rings of the prolyl residues act as binding sites and form "hydrophobic stacks" with the galloyl rings of polyphenols (*17, 25*). Ethanol addition, by its influence on water cohesion and hydrogen-bonding properties (*35*), may weaken these interactions. Experiments were repeated in a pH 3.5 and 100 mM NaCl aqueous solution with 12% ethanol. The SAXS spectrum of protein II-1 alone (3 mg/mL) in this solvent was close to that obtained in the absence of ethanol (results not shown). Accordingly, the average structure of the protein II-1 is not sensitive to such solvent changes. The spectra of protein II-1 (initial concentration 3 mg/mL as above) in presence of EGCG (up to 2.51 mg/mL) did not show the excess scattering presented in **Figure 5**. Instead, they remained identical with those of the pure protein solution. Accordingly, the addition of ethanol disrupted the aggregation mechanism that was observed in aqueous NaCl solutions.

Effect of PRP Glycosylation on Their Aggregation with EGCG. The results that have been obtained here with the glycosylated PRP II-1 and EGCG are in contrast with those found previously with the nonglycosylated protein IB-5 (*29*). Interactions between IB5 and EGCG were studied by means of DLS, circular dichroism (CD), and isothermal titration microcalorimetry (ITC). Results indicated that the interaction mechanism was dependent on protein concentration. At low protein concentrations (0.2 mg/mL) a three-stage mechanism was evidenced, in agreement with that proposed by other authors for the interactions between denaturated proteins/peptides and flavan-3-ols (*14, 17*). Below a given EGCG/IB5 ratio, ITC and CD experiments evidenced EGCG/protein interactions (binding) but no aggregate formed. Aggregation, evidenced through DLS experiments, occurred as soon as the protein and EGCG solutions were mixed, provided that the EGCG concentration exceeded a threshold that was between 0.22 and 0.44 mg/mL (corresponding to EGCG/protein molar ratios between 18 and 36). For intermediate EGCG concentrations, aggregation first led to the formation of metastable dispersions of particles. Increasing the EGCG content finally led to phase separation (haze formation). At high IB5 concentrations, aggregation was attributed to direct bridging of two proteins by EGCG monomers. Increasing IB5 concentration strongly decreased the thresholds for aggregation and phase separation: at 1 mg/mL, aggregation was observed for an EGCG concentration of 0.2 mg/mL (corresponding to a molar ratio of 3 EGCG/protein). It was attributed to direct bridging between the protein and the flavan-3-ol.

The common features of EGCG-induced aggregation for IB5 and for II-1 are that, in both cases, there is a threshold in EGCG/protein beyond which EGCG causes the proteins to aggregate. The first difference is that, for II-1, aggregation takes place only at rather high protein concentrations ($\geq$1 mg/mL) and for higher EGCG/protein ratios (molar ratio of 80 for a II-1 concentration of 1 mg/mL). The second difference is that, for II-1, the aggregates retain a finite size instead of growing to macroscopic sizes. All these results consistently point out an effect of protein glycosylation on its aggregation and precipitation behavior in the presence of EGCG. The glycosyl moieties are strongly hydrophilic, in contrast to the proline residues of the protein backbone. This may first influence protein affinity for EGCG, depending on the location of the glycosyl residue with regard to interaction sites. Second, glycosylation may create steric hindrance that limits the extent of protein bridging by EGCG. This may be the cause of the higher EGCG concentrations that are needed to produce aggregation. Moreover, when aggregates form, these glycosyl moieties must remain exposed to the aqueous phase, at the outer surface of the aggregates. This may be the reason for the limited size of the aggregates. Thus the effect of glycosylation can explain both the delay in the onset of aggregation (compared with nonglycosylated proteins) by EGCG and the limitation of aggregate radii to approximately the size of a protein chain. Further experiments will be needed to get more precise data on the aggregation mechanisms and on the aggregate structure.

Interactions between II-1 and Condensed Tannins. Interactions between proline-rich proteins and tannins (hydrolyzable or condensed tannins) have been shown to increase with the polymerization degree of the latter. This is attributed to enhanced affinity between tannins and proteins, along with the occurrence of multiple bonding between the two species (*21, 25, 42, 47*). In addition, increasing the flavan-3-ol size likely favors intermolecular bridging between proteins. Major polyphenols in wines, responsible for astringency, are flavan-3-ol polymers. It was thus of importance here to check II-1 behavior in the presence of higher molecular weight polyphenols. II-1/tannin aggregation was studied by DLS at low protein concentration (0.2 mg/mL) and with two condensed grape seed tannin fractions of mean degree of polymerization 4 and 15, respectively.

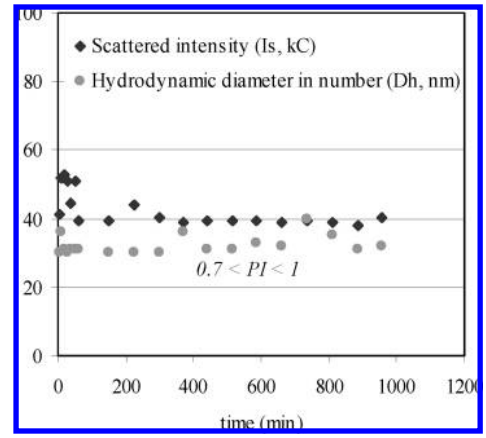

Figure 6. Evolution of the mDP 4 tannin/II-1 mixture as a function of time in 1% ethanol, for a tannin concentration of 0.06 mg/mL and a protein concentration of 0.2 mg/mL. I_s, normalized scattered intensity (kC); D_h, mean hydrodynamic diameter weighted according to the number (nanometers); *PI*, polydispersity index of the suspension. Results evidenced immediate aggregation between tannins and II-1, leading to the formation of polydisperse colloidal particles with a finite size. The aggregates remained stable (no phase separation) over the whole experiment duration.

The lowest molecular weight fraction was tested first, at a tannin concentration of 0.06 g/L and at a low ethanol percentage. Mixing the tannin and the protein solutions resulted in an abrupt rise of the scattered intensity to a value 40 times higher than the sum of the individual solutions. This clearly indicated interactions between the two species, leading to the formation of colloidal aggregates. The suspension did not change during the experiment duration: neither the scattered intensity nor the aggregate mean hydrodynamic diameter evolved, and no phase separation occurred (**Figure 6**). Once formed, aggregates remained stable. Cumulant analysis showed that these aggregates were highly polydisperse (*PI* between 0.7 and 1) and had a mean hydrodynamic diameter of 170 nm. Contin analysis indicated that most of the particles were much smaller since the average diameter weighted according to the number was on the order of 30 nm. For comparison, the same experiment was performed with the nonglycosylated protein IB5. A phase separation, indicating enlarged aggregation, was immediately observed. Thus, protein glycosylation still prevented aggregation, even though the increase in the polyphenol molecular weight favored tannin/II-1 aggregation.

Interactions of the highest mDP fraction were studied in 2% and 12% (v/v) ethanol with tannin concentrations between 0.015 and 1 mg/mL. Aggregation was always observed and led in most cases to the formation of finite and metastable colloidal particles, as before (**Figures 7** and **8**). As observed with EGCG, ethanol affects tannin/II-1 interactions and/or the stability of the flavanol/protein aggregates. Suspensions formed in 12% ethanol always scattered less light than those formed in 2% ethanol. This could not be attributed to a

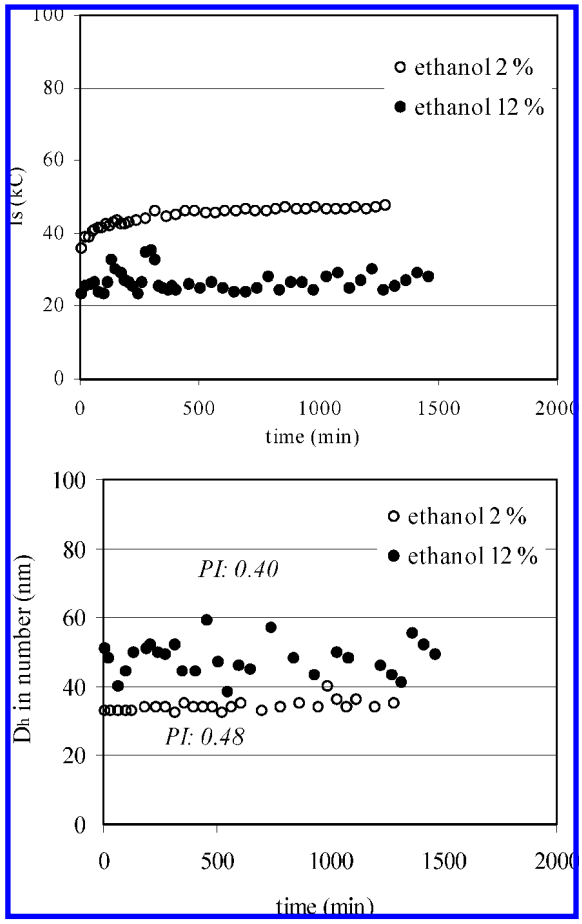

Figure 7. Evolution of mDP 15 tannin/II-1 mixtures as a function of time followed by DLS in 2% and 12% ethanol. Results are given for a tannin concentration of 0.06 mg/mL and a protein concentration of 0.2 mg/mL. I_s, scattered intensity in kilocounts; D_h, mean hydrodynamic diameter, number average (nanometers); *PI*, polydispersity indexes of the suspensions. As for the mDP 4 tannins, results evidenced immediate aggregation between tannins and II-1, leading to the formation of polydisperse colloidal particles with a finite size. The aggregates remained stable (no phase separation) over the whole experiment duration.

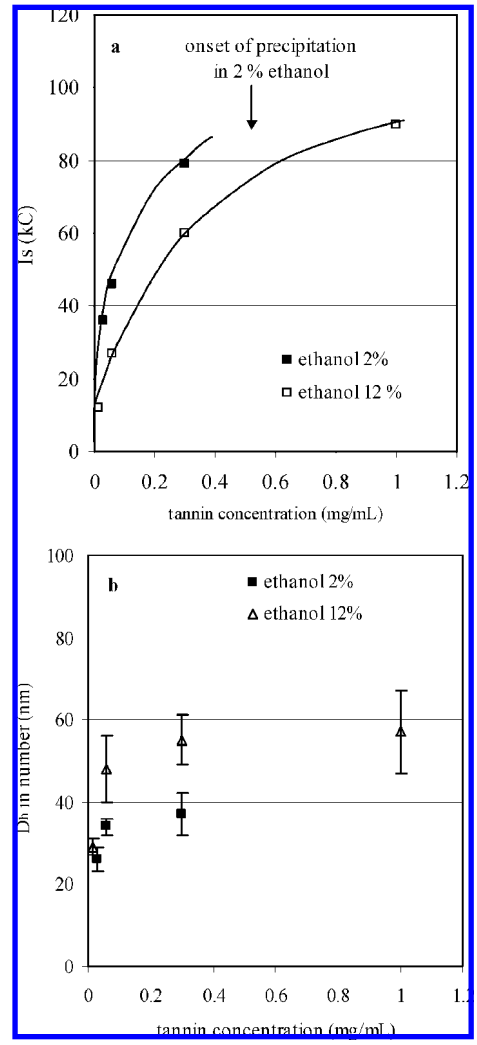

Figure 8. Interactions between grape seed tannins (mDP 15) and the glycosylated PRP in 2% and 12% ethanol aqueous solutions: influence of tannin concentration on (**a**) mean scattering intensity I_s of the suspensions, in kilocounts, and (**b**) mean D_h hydrodynamic diameter (number average) of the aggregates. The protein concentration was held at 0.2 mg/mL. A phase separation was observed for a mDP 15 concentration of 0.6 mg/mL in 2% ethanol, whereas aggregates in 12% ethanol remained stable and of finite size for tannin concentrations up to 1 mg/mL.

difference in the mean aggregate size or polydispersity index of the suspensions and may indicate that more aggregates are formed between tannins and II-1 at low ethanol contents. Furthermore, ethanol addition prevented the phase separation observed at high tannin/protein ratios. Indeed, a precipitation occurred for a mDP 15 concentration of 0.6 mg/mL and in the 2% ethanol solvent. Such a phase separation did not happen in 12% ethanol, even when tannin concentration was raised to 1 mg/mL. Such an influence of ethanol on polyphenol/protein interactions and precipitation was already reported by Siebert and Lynn (*46*) for gliadin/tannic acid systems.

The difference in II-1 and IB-5 behaviors toward polyphenol precipitation is in accordance with that found by Lu and Bennick (*27*). These authors compared the ability of acidic, basic, and glycosylated PRPs to precipitate condensed tannins (quebracho extract) and tannic acid. They found that both tannins were only slightly precipitated by glycosylated PRPs, whereas basic PRPs were very effective in precipitating them. Moreover, glycosylated PRPs that were deglycosylated exhibited the same behavior toward precipitation as basic PRPs. The present results indicate that these differences between the two PRP classes are not necessarily related to distinct affinities toward condensed tannins: glycosylated PRPs are in fact effective in binding tannins. However, these interactions do not necessarily result in precipitation. Indeed, Bacon and Rhodes (*5, 48*), who studied interactions between salivary PRPs and different hydrolyzable tannins at a molecular level and by means of a competition assay, concluded that all the PRP classes present similar affinities toward these polyphenols.

As stated before, astringency is attributed to a precipitation of PRPs by tannins. This precipitation may reduce the lubricative properties of saliva, either through a reduction of saliva viscosity, or possibly the aggregates themselves can produce friction between oral tissues (*7–12, 49*). Glycosylated PRPs, which have been implicated in the oral epithelium lubrication (*19*), were shown here to resist precipitation. However, they form complexes with tannins and this complexation likely modifies their rheological properties. Moreover, this complexation led to the formation of small and finite particles that might produce friction-based sensation.

ACKNOWLEDGMENT

It is a pleasure for us to thank Cyril Rochas for guidance and assistance in the SAXS experiments. The authors also thank Jean-Paul Mazauric and Jean-Marc Souquet for tannin purification and characterization.

LITERATURE CITED

(1) Bennick, A. Interaction of plant polyphenol with salivary proteins. *Crit. Rev. Oral Biol. Med.* **2002**, *13*, 184–196.
(2) Mehansho, H.; Butler, L. G.; Carlson, D. M. Dietary tannins and salivary proline-rich proteins: Interactions, induction, and defense mechanisms. *Annu. Rev. Nutr.* **1987**, *7*, 423–440.
(3) Bennick, A. Salivary proline-rich proteins. *Mol. Cell. Biochem.* **1982**, *45*, 83–99.
(4) Edgar, W. M. Saliva: its secretion, composition and functions. *Br. Dent. J.* **1992**, *172*, 305–312.
(5) Bacon, J. R.; Rhodes, M. J. C. Binding affinity of hydrolyzable tannins to parotid saliva and to proline-rich proteins derived from it. *J. Agric. Food Chem.* **2000**, *48*, 838–843.
(6) ASTM Standard definitions of terms relating to sensory evaluation of materials and products. In *Annual Book of ASTM Standards*; American Society of Testing and Materials: Philadelphia, PA, 1989; p 2.
(7) De Wijk, R.; Prinz, J. Mechanisms underlying the role of friction in oral texture. *J. Texture Stud.* **2006**, *37*, 413–427.
(8) Brossaud, F.; Cheynier, V.; Noble, A. Bitterness and astringency of grape and wine polyphenols. *Aust. J. Grape Wine Res.* **2001**, *7*, 33–39.
(9) Clifford, M. N. Astringency. In *Phytochemistry of fruits and vegetables*; Tomas-Barberan, F., Robins, R., Eds.; Clarendon Press: Oxford, U.K., 1997; pp 87−108.
(10) Green, B. G. Oral astringency: a tactile component of flavor. *Acta Psychol.* **1993**, *84*, 119–125.
(11) Smith, A. K.; June, H.; Noble, A. C. Effects of viscosity on the bitterness and astringency of grape seed tannin. *Food Qual. Preference* **1996**, *7*, 161–6.
(12) Bate-Smith, E. C. Astringency in foods. *Food* **1954**, *23*, 124.
(13) Jöbstl, E.; Howse, J. R.; Fairclough, J. P. A.; Williamson, M. P. Noncovalent cross-linking of casein by epigallocatechin gallate characterized by single molecule force microscopy. *J. Agric. Food Chem.* **2006**, *54*, 4077–4081.
(14) Jöbstl, E.; O'Connell, J.; Fairclough, J. P. A.; Williamson, M. P. Molecular model for astringency produced by polyphenol/protein interactions. *Biomacromolecules* **2004**, *5*, 942–949.
(15) Azen, E. A.; Amberger, E.; Fisher, S.; Prakobphol, A.; Niece, R. L. PRB1, PRB2, and PRB4 coded polymorphisms among human salivary concanavalin-A binding, II-1, and Po proline-rich proteins. *Am. J. Hum. Genet.* **1996**, *58*, 143–153.
(16) Chan, M.; Bennick, A. Proteolytic processing of a human salivary proline-rich protein precursor. *Eur. J. Biochem.* **2001**, *268*, 3423–3431.
(17) Charlton, A.; Baxter, N. J.; Khan, M. L.; Moir, A. J. G.; Haslam, E.; Davis, A. P.; Williamson, M. P. Polyphenol/peptide binding and precipitation. *J. Agric. Food Chem.* **2002**, *50*, 1593–1601.
(18) Douglas, C. W. I. Bacterial-protein interactions in the oral cavity. *Adv. Dent. Res.* **1994**, *8*, 254–262.
(19) Hatton, M. N.; Loomis, R. E.; Levine, M. J.; Tabak, L. A. Masticatory lubrification. The role of carbohydrate in the lubricating property of a salivary glycoprotein-albumin complex. *Biochem. J.* **1985**, *230*, 817–820.
(20) Siebert, K. J.; Lynn, P. Y. Effect of protein-polyphenol ratio on the size of haze particles. *J. Am. Brew. Chem.* **2000**, *58*, 117–123.
(21) Sarni-Manchado, P.; Deleris, A.; Avallone, S.; Cheynier, V.; Moutounet, M. Analysis and characterization of wine condensed tannins precipitated by proteins used as fining agent in enology. *Am. J. Enol. Vitic.* **1999**, *50*, 81–86.
(22) Sarni-Manchado, P.; Cheynier, V.; Moutounet, M. Interactions of grape seed tannins with salivary proteins. *J. Agric. Food Chem.* **1999**, *47*, 42–47.
(23) McManus, J. P.; Davis, K. G.; Beart, J. E.; Gaffney, S. H.; Lilley, T. E.; Haslam, E. Polyphenol interactions. Part I. Introduction: Some observations on the reversible complexation of polyphenols with proteins and polysaccharides. *J. Chem. Soc., Perkin Trans. II* **1985**, *142*, 9–1438.
(24) Hagerman, A. E.; Rice, M. E.; Richard, N. T. Mechanisms of protein precipitation from two tannins, pentagalloylglucose and epicatechin 16 (4−8)catechin (procyanidin). *J. Agric. Food Chem.* **1998**, *46*, 2590–2595.
(25) Baxter, N. J.; Lilley, T. H.; Haslam, E.; Williamson, M. P. Multiple interactions between polyphenols and a salivary proline-rich protein repeat result in complexation and precipitation. *Biochemistry* **1997**, *36*, 5566–5577.
(26) Sarni-Manchado, P.; Cheynier, V. Study of noncovalent complexation between catechin derivates and peptides by electrospray ionization-mass spectrometry (ESI-MS). *J. Mass Spectrom.* **2002**, *37*, 609–616.
(27) Lu, Y.; Bennick, A. Interaction of tannin with human salivary proline-rich proteins. *Arch. Oral Biol.* **1998**, *43*, 717–728.
(28) Pascal, C.; Bigey, F.; Ratomahenina, R.; Boze, H.; Moulin, G.; Sarni-Manchado, P. Overexpression and characterization of two human salivary proline-rich proteins. *Protein Expression Purif.* **2006**, *47*, 524–532.
(29) Pascal, C.; Poncet-Legrand, C.; Imberty, A.; Gautier, C.; Sarni-Manchado, P.; Cheynier, V.; Vernhet, A. Interactions between a non glycosylated human proline-rich protein and flavan-3-ols are affected by protein concentration and polyphenol/protein ratio. *J. Agric. Food Chem.* **2007**, *55*, 4895–4901.
(30) Prieur, C.; Rigaud, J.; Cheynier, V.; Moutounet, M. Oligomeric and polymeric procyanidins from grape seeds (*Vitis vinifera*). *Phytochemistry* **1994**, *36*, 781–784.
(31) Souquet, J.-M.; Cheynier, V.; Brossaud, F.; Moutounet, M. Polymeric proanthocyanidins from grape skins. *Phytochemistry* **1996**, *43*, 509–512.
(32) Flanzy, C. *Oenologie - Fondements scientifiques et technologiques*; Technique et Documentation ed.; Lavoisier: Paris, 1998; p 1311.
(33) Doco, T.; O'Neill, M. A.; Pellerin, P. Determination of the neutral and acidic glycosyl-residue compositions of plants polysaccharides by GC-EI-MS analysis of the trimethylsilyl methyl glycoside derivatives. *Carbohydr.Polym.* **2001**, *46*, 249–259.
(34) Harris, P. J.; Henry, R. J.; Blakeney, A. B.; Stone, B. A. An improved procedure for the methylation analysis of oligosaccharides and polysaccharides. *Carbohydr. Res.* **1984**, *127*, 59.
(35) Poncet-Legrand, C.; Cartalade, D.; Putaux, J. L.; Cheynier, V.; Vernhet, A. Flavan-3-ols self-aggregation in model ethanolic solutions: incidence of polyphenol structure, concentration, ethanol content and ionic strength. *Langmuir* **2003**, *19*, 10563–10572.
(36) Gal, J. Y.; Fovet, Y.; Adib-Yadzi, M. About a synthetic saliva for in vitro studies. *Talanta* **2001**, *53*, 1103–1115.
(37) Provencher, S. W. A constrained regularization method for inverting data represented by linear algebraic or integral equations. *Comput. Phys. Commun.* **1982**, *27*, 213–227.
(38) Porod, G. In *Small angle X-ray scattering*; Glatter, E. O., Kratky, O., Eds.; Academic Press: London, 1982.
(39) Guinier, A.; Fournet, G. *Small angle scattering of X-rays*; Wiley: New York, 1955.
(40) Pérez, J.; Vachette, P.; Russo, D.; Desmadril, M.; Durand, D. Heat-induced unfolded of neocarzinostatin, a small all-b protein investigated by small-angle X-ray scattering. *J. Mol. Biol.* **2001**, *308*, 721–743.
(41) Moncoq, K.; Broutin, I.; Craescu, C. T.; Vachette, P.; Ducruix, A.; Durand, D. SAXS study of the PIR domain from the Grb molecular adaptator: a natively unfolded protein with a transient structure primer? *Biophys. J.* **2004**, *87*, 4056–4064.
(42) Haslam, E. *Practical Polyphenolics*; Cambridge University Press: Cambridge, U.K., 1998.
(43) Artz, W. E.; Bishop, P. D.; Dunker, A. K.; Schanus, E. G.; Swanson, B. G. Interaction of synthetic proanthocyanidin dimer and trimer with bovine serum albumin and purified bean globulin fraction G-1. *J. Agric. Food Chem.* **1987**, *35*, 417–421.

(44) Oh, H.-I.; Hoff, J. E. pH dependence of complex formation between condensed tannins and proteins. *J. Food Sci.* **1987**, *52*, 1267–1269.

(45) Simon, C.; Barathieu, K.; Laguerre, M.; Schmitter, J. M.; Fouquet, E.; Pianet, I.; Dufourc, E. J. Three.dimensional structure and dynamics of wine tannin-saliva protein complexes. A multitechnique approach. *Biochemistry* **2003**, *42*, 10385–10395.

(46) Siebert, K.; Lynn, P. Effects of alcohol and pH on protein-polyphenol haze intensity and particle size. *J. Am. Soc. Brew. Chem.* **2003**, *61*, 88–93.

(47) Poncet-Legrand, C.; Gautier, C.; Cheynier, V.; Imberty, A. Interactions between flavan-3-ols and poly(L-proline) studied by isothermal titration calorimetry: effect of the tannin structure. *J. Agric. Food Chem.* **2007**, *55*, 9235–9240.

(48) Bacon, J. R.; Rhodes, M. J. C. Development of a competition assay for the evaluation of the binding of human parotid salivary proteins to dietary complex phenols and tannins using a peroxidase-labeled tannin. *J. Agric. Food Chem.* **1998**, *46*, 5083–5088.

(49) de Freitas, V.; Carvalho, E.; Mateus, N. Study of carbohydrate influence on protein-tannin aggregation by nephelometry. *Food Chem.* **2003**, *81*, 503–509.

Received for review March 13, 2008. Revised manuscript received May 19, 2008. Accepted May 25, 2008.

JF800790D